THESIS FOR THE DEGREE OF LICENTIATE OF ENGINEERING IN MATERIALS SCIENCE

Additive Manufacturing of High-Silicon Steel Soft Magnetic Material

MUKESH MURALI

Department of Mechanical Engineering

CHALMERS UNIVERSITY OF TECHNOLOGY

Gothenburg, Sweden 2026

Additive Manufacturing of High-Silicon Steel Soft Magnetic Material

MUKESH MURALI

Licentiate Thesis at Chalmers University of Technology
Department of Mechanical Engineering
Chalmers University of Technology
SE-412 96 Gothenburg
Sweden
Tel: +46 (0)31 772 1000

Chalmers Digitaltryck
Gothenburg, Sweden 2026

Additive Manufacturing of High-Silicon Steel Soft Magnetic Material

Mukesh Murali

Department of Mechanical Engineering
Chalmers University of Technology

Abstract

Soft magnetic materials play a critical role in electric motors and transformers, where high efficiency and low energy losses are essential. High-silicon steels (Fe-6.5 wt.% Si) offer superior soft magnetic properties but are difficult to process using conventional manufacturing due to their inherent brittleness. Powder bed fusion-laser beam (PBF-LB) provides a promising alternative by enabling near-net-shape fabrication and microstructural control.

This thesis investigates the influence of PBF-LB processing parameters, scan strategies, and heat treatments on the evolution of microstructure and the magnetic, mechanical, and electrical properties of high-silicon steel soft magnetic material. The first part of the thesis focuses on the influence of process parameters and heat treatment on the microstructure and multi-functional properties. A wide parameter space of laser power and scan speed was systematically explored to identify processing regimes associated with lack-of-fusion defects, keyhole-induced porosity, and near-full densification. Magnetic characterization revealed pronounced anisotropic behavior relative to the build orientation, while post-processing annealing treatments significantly enhanced soft magnetic performance by reducing coercivity and promoting grain growth as well as microstructural homogenization. The second part of the thesis investigates the influence of laser scan rotation on melt pool behavior, grain structure, and multi-functional properties. Variations in scan rotation altered melt pool overlap and grain morphology, leading to pronounced differences in texture, magnetic anisotropy, hardness, and electrical resistivity. A 90° scan rotation promoted the formation of coarse, textured columnar grains and superior soft magnetic properties, whereas annealing consistently reduced coercivity and anisotropy across all scan strategies. The results demonstrate that careful control of both energy input and laser path design provides an effective route for tailoring the microstructure and coupled properties of additively manufactured high-silicon steel, enabling site-specific optimization for energy-efficient electrical machine applications.

Key-words: Additive manufacturing (AM); Powder bed fusion-laser beam (PBF-LB); High-silicon steel; Soft magnetic materials; Scan strategies.

Preface

This licentiate thesis is based on the work performed in the Department of Mechanical Engineering at Chalmers University of Technology from September 2023 to June 2026. The work has been carried out with Assistant Professor Varun Chaudhary as the main supervisor and Professor Eduard Hryha as co-supervisor, with Professor Uta Klement as examiner. The work was funded by the Area of Advance (AoA) Production at Chalmers University of Technology. Support from the Centre for Additive Manufacture -Metal (CAM^2), supported by the Swedish Governmental Agency for Innovation Systems (VINNOVA), is greatly acknowledged.

List of the appended papers:

Paper 1: Energy density-driven microstructure and functional properties of Fe-6.5 wt.% Si steel processed by powder bed fusion-laser beam

Mukesh Murali, Gokul Babu, Eduard Hryha, Varun Chaudhary

Manuscript

Paper 2: Laser path engineering of microstructure and multi-properties in additively manufactured high-silicon steel

Mukesh Murali, Eduard Hryha, Uta Klement, Varun Chaudhary

Manuscript

Contribution to the appended papers:

Paper 1: The author jointly planned the work with the co-authors and supervisors, conducted most of the experimental work and data analysis, except the melt pool analysis and magnetic properties of the samples printed using high-throughput method. The manuscript was drafted by the author which was then subsequently revised in collaboration with the co-authors.

Paper 2: The author jointly planned the work with the co-authors and supervisors, conducted all experimental work and data analysis, and drafted the manuscript. The manuscript was subsequently revised in collaboration with the co-authors.

Table of Contents

1. Introduction

The ongoing era of electrification is driving a rapid expansion of electric motors and transformer systems across automotive, aerospace, renewable energy, and industrial sectors [1]. As these technologies become increasingly central to modern energy infrastructure, there is a growing demand for electromagnetic devices that operate with higher efficiency, reduced losses, and improved reliability [1-3]. Enhancing system efficiency is essential not only for performance gains but also for reducing energy consumption and environmental impact. The efficiency of electric motors and transformers is strongly influenced by the properties of their magnetic core materials, placing soft magnetic materials at the core of technological innovation in this field [4-7]. Ideal soft magnetic materials must combine high magnetic permeability, low coercivity, minimal hysteresis and eddy-current losses, and sufficient mechanical stability for manufacturing and integration into complex components [3, 8]. As operating frequencies and power densities continue to rise, the need for advanced soft magnetic materials with optimized functional properties becomes increasingly critical [2, 9].

Iron-silicon alloys with higher silicon content have emerged as promising candidate for such applications [10]. In particular, Fe-6.5 wt.% Si exhibits superior magnetic performance compared to conventional electrical steels, including higher electrical resistivity, lower core losses, and near-zero magnetostriction [9-11]. These properties make it especially attractive for high-frequency and high-efficiency motor and transformer applications [10]. Despite these advantages, the widespread adoption of Fe-6.5 wt.% Si remains limited by significant processing challenges. A key limitation of Fe-6.5 wt.% Si is its pronounced brittleness at room temperature, which arises from the higher silicon concentration [12, 13]. This brittleness restricts the use of traditional thermomechanical processing routes such as rolling and forming, complicating the production of bulk or geometrically complex components [9]. Industrial solutions, such as the chemical vapor deposition (CVD) based silicon enrichment process developed by JFE Steel Corporation, have been introduced to address this issue [14, 15]. However, these approaches involve high production costs, complex processing steps, and limited scalability, particularly for customized or three-dimensional component geometries [9].

Additive manufacturing (AM) offers an alternative route capable of overcoming many of these limitations [7, 10, 16, 17]. Powder bed fusion-laser beam (PBF-LB), in particular, enables near-net-shape fabrication directly from powder feedstock, allowing for complex geometries [18, 19]. Additionally, the extremely high cooling rates associated with PBF-LB significantly

affect solidification behavior and microstructural evolution, offering opportunities for microstructural refinement and property tailoring in high-silicon steels [10, 20]. Nevertheless, realizing the full potential of PBF-LB for Fe-6.5 wt.% Si requires a detailed understanding of how processing parameters, in particular scanning strategies, and post-processing treatments influence microstructure and functional properties. Establishing these process-structure-property relationship is essential for enabling reliable, scalable, and application-ready AM of high-silicon soft magnetic materials for next-generation electric motor and transformer systems. This thesis focuses on systematically exploring the relationships between PBF-LB processing parameters, in particular scan strategies, and post-processing treatments, and their combined effects on the microstructure and functional properties of Fe-6.5 wt.% Si soft magnetic material.

1.1. Research objectives

The overall objective of this thesis is to investigate how AM process parameters, post-processing treatments, and resulting microstructural features influence the magnetic, mechanical, and electrical properties of high-silicon soft magnetic steel. These objectives are addressed through the following research questions (RQs):

RQ1: What is the effect of PBF-LB process parameters on the microstructure and functional properties (magnetic, mechanical and electrical properties) of Fe-6.5 wt.% Si alloy?

RQ2: How do variations in laser scan strategies affect the microstructural evolution and functional properties of Fe-6.5 wt.% Si alloy?

RQ3: What is the impact of post-processing on the microstructure and functional properties of Fe-6.5 wt.% Si alloy?

Paper 1 addresses RQ1 and RQ3, while Paper 2 addresses RQ2 and RQ3.

2. Soft magnetic materials

Soft Magnetic Materials (SMMs) are characterized by low coercivity (typically < 1000 A/m according to IEC 60404-1) [21], enabling easy magnetization and demagnetization under low applied magnetic fields. Their key attributes include low coercivity, high magnetic permeability, high saturation magnetization, low core losses, and a sufficiently high Curie temperature, making them indispensable for applications such as electric motors, generators, transformers, and power electronic components [22].

To meet the increasing demands of modern electrical machines such as higher efficiency, greater power density, and operations at elevated speeds and temperatures, soft magnetic materials must also exhibit high electrical resistivity, adequate mechanical strength, and effective thermal conductivity [23]. Several material systems are used to address these requirements, including Fe-Si, Fe-Co, Fe-Ni alloys, low-carbon steels, soft magnetic composites, and ferrites [7, 10, 24-29]. Among these, silicon based electrical steel (with Si < 4 wt.%) are widely used due to their favorable balance of magnetic performance, cost, and availability [5, 9]. These materials are typically manufactured as laminated sheets through conventional processes such as rolling and stacking of coated laminations to suppress eddy-current losses, making them well suited for low-frequency applications [30, 31]. However, at higher operating frequencies, their relatively modest electrical resistivity leads to increased core losses, which reduces energy efficiency and limits their suitability for high-frequency applications [9].

2.1. High-silicon steel (Fe-6.5 wt.% Si)

Increasing silicon content in electrical steels significantly enhances functional performance by increasing electrical resistivity, reducing iron losses, and lowering magnetostriction [11]. In particular, Fe-6.5 wt.% Si exhibits low coercivity, high magnetic permeability, low core losses, and near-zero magnetostriction, making it especially suitable for high-frequency transformers, reactors, and high-speed motor applications [11]. The performance of Fe-6.5 wt.% Si soft magnetic alloys is governed by control of iron losses through deliberate manipulation of microstructure and crystallographic texture [32, 33]. Iron losses consist primarily of hysteresis and eddy-current components, both of which are strongly influenced by grain size, grain orientation, impurity content, and electrical resistivity [34, 35]. Hysteresis losses can be minimized by promoting coarse grains with favorable crystallographic orientation, particularly a high fraction of ⟨001⟩ grains, which facilitate domain wall motion, and reduce coercivity [34].

The higher silicon content increases electrical resistivity, thereby reducing eddy-current losses, but also introduces processing challenges related to brittleness [11].

2.2. Challenges with the production of high-silicon steel

Fe-Si electrical steels undergo distinct structural changes as the silicon content increases[11, 36]. At low silicon concentrations, the alloy consists of a disordered A2 body-centered cubic (bcc) α-Fe(Si) solid solution [36, 37]. When the silicon content increases, ordering begins to develop leading to the formation of the B2 (FeSi) and $D0_3$ (Fe_3Si) ordered phases [36, 37]. The presence of these ordered phases significantly strengthens the material through strong interactions with dislocations, but this strengthening is accompanied by a substantial increase in brittleness [38, 39]. As a result, producing Fe-6.5 wt.% Si soft magnetic materials using conventional fabrication routes such as rolling becomes highly challenging. To overcome this limitation, industrial processes such as CVD-based silicon enrichment have been developed (JFE steels), enabling the production of high-silicon electrical steels for specialized applications [14, 15]. While these steels offer superior functionality, their complex processing routes and associated costs limit large-scale adoption. Consequently, the development of alternative manufacturing approaches capable of producing high-silicon soft magnetic material in a scalable and cost-effective manner remains an active area of research.

3. Powder Bed Fusion - Laser Beam (PBF-LB)

Powder bed fusion is an AM technique in which a focused energy source selectively melts powder material in a layer-wise manner to build three-dimensional components [40, 41]. In the PBF-LB process, a focused laser beam scans across a powder bed and locally fuses metal particles according to the digital layer information derived from a computer-aided design (CAD) model, typically converted into an STL file. Owing to its capability to fabricate complex metallic parts with high dimensional accuracy and near-net-shape geometry, PBF-LB has become one of the most widely adopted metal additive manufacturing technologies [42].

3.1. Working principle of PBF-LB

Figure 1 illustrates the working principle of the PBF-LB process as implemented in an EOS M100 system. The process begins with a powder dispenser supplying a thin layer of alloy powder onto the build area, which is uniformly spread across the powder bed by a recoater blade. The build platform is positioned slightly below the recoating plane and moves downwards incrementally after each layer is processed, defining the layer thickness (typically 20-60μm). A laser source, guided by laser optics, emits a focused laser beam that selectively scans the powder bed according to a predefined scan path derived from the digital design. The laser locally melts the powder, forming a melt pool that solidifies rapidly to create consolidated material. After each layer is completed, excess powder is collected in the powder collector, while the recoater deposits a fresh powder layer for the next scanning cycle. This layer-by-layer sequence continues until the three-dimensional component is fully built. The schematic highlights key elements of the PBF-LB process, including powder delivery, recoating, selective melting, and vertical movement of the build platform, which together enable precise fabrication of complex metallic components.

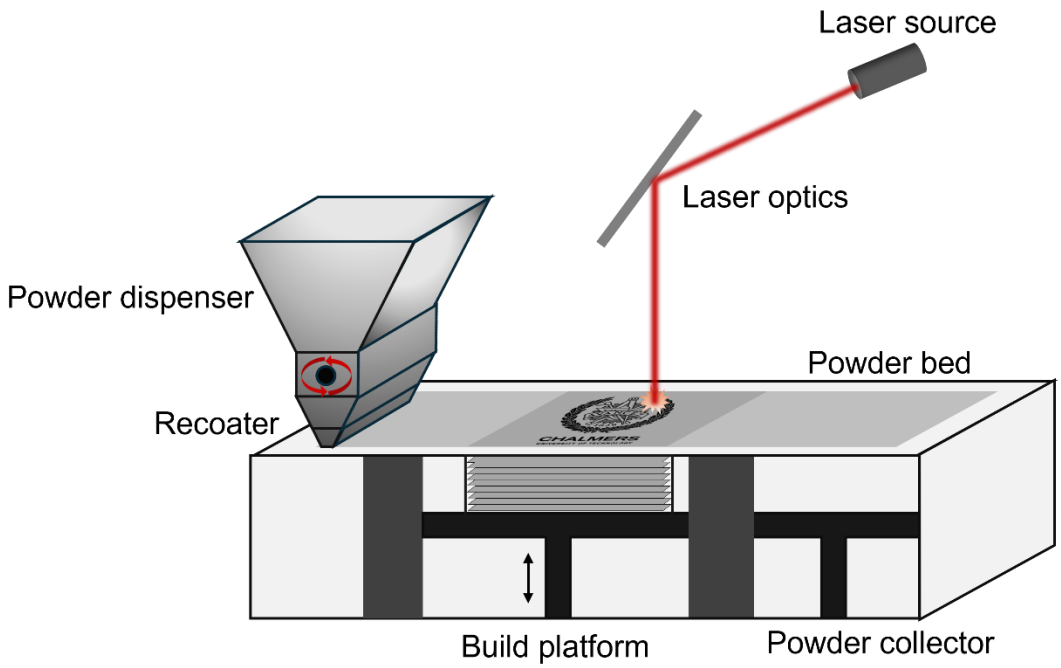

Figure 1: Schematic of the PBF-LB process in EOS M100 system. Key components of the powder bed formation and laser melting are shown.

3.2. Process parameters in PBF-LB

In the PBF-LB process, the printing process is governed by a set of interdependent process parameters that collectively control the energy input and consolidation behavior [43]. Even though there are several parameters associated, only a few are considered for the optimization process. Laser power (P) and scan speed (υ) determine the local heat input, while layer thickness (t) and hatch distance (h) define the volume of material processed and the degree of overlap between adjacent scan tracks [19, 44]. These parameters are commonly combined into volumetric energy density (VED) [19, 45], as given in Equation 1.

$$VED = \frac{P}{v \cdot h \cdot t} \tag{1}$$

where P is in W, υ in mm/s, h and t in mm and VED in J/mm^3. As illustrated in **Figure 2**, the resulting VED directly influences melt pool width and penetration depth, affecting interlayer bonding, re-melting behavior, and solidification dynamics [42]. Consequently, VED plays a central role in controlling the thermal history, density, defect formation, and microstructural evolution during layer-by-layer fabrication [45].

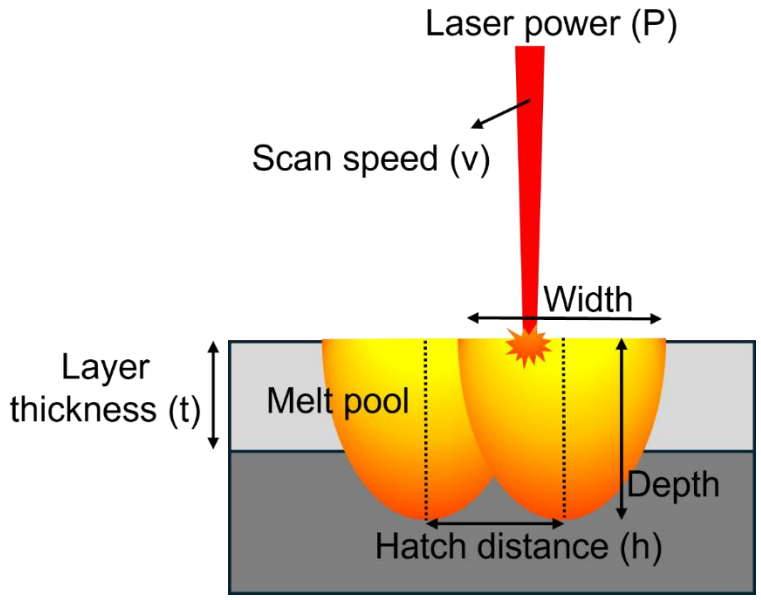

Figure 2: Schematic of PBF-LB printing process illustrating the melt pool formation and the key governing process parameters.

3.3. Scan strategies in PBF-LB

The scan strategy in the PBF-LB process defines the path followed by the laser beam while melting the powder bed. It plays a key role in controlling heat distribution, melt pool overlap, and microstructural evolution [46, 47]. **Figure 3** illustrates the used scan strategies investigated in this work. In the unidirectional scan strategy (**Figure 3a**), the laser moves in a single direction for all scan tracks whereas in bidirectional scan strategy (**Figure 3b**), the scanning direction is alternating between successive tracks. The laser scan direction can be changed between successive layers which can lead to different microstructures. The bidirectional scan strategy with no scan rotation between layers (**Figure 3c**), results in repeated scanning along the same orientation throughout the build. A 45° scan rotation (**Figure 3d**) rotates the scan direction by 45° after each layer, promoting more uniform heat distribution and reducing directional anisotropy. Similarly, a 67° scan rotation (**Figure 3e**) further disrupts the alignment of melt pools and grain growth across layers [48]. Finally, a 90° scan rotation (**Figure 3f**) alternates the scan direction orthogonally between the layers, significantly altering thermal gradients and solidification patterns [48]. These scan strategies influence many features including melt pool geometry and grain morphology, and thereby strongly affect the mechanical, magnetic, and electrical properties of the printed material [48-50].

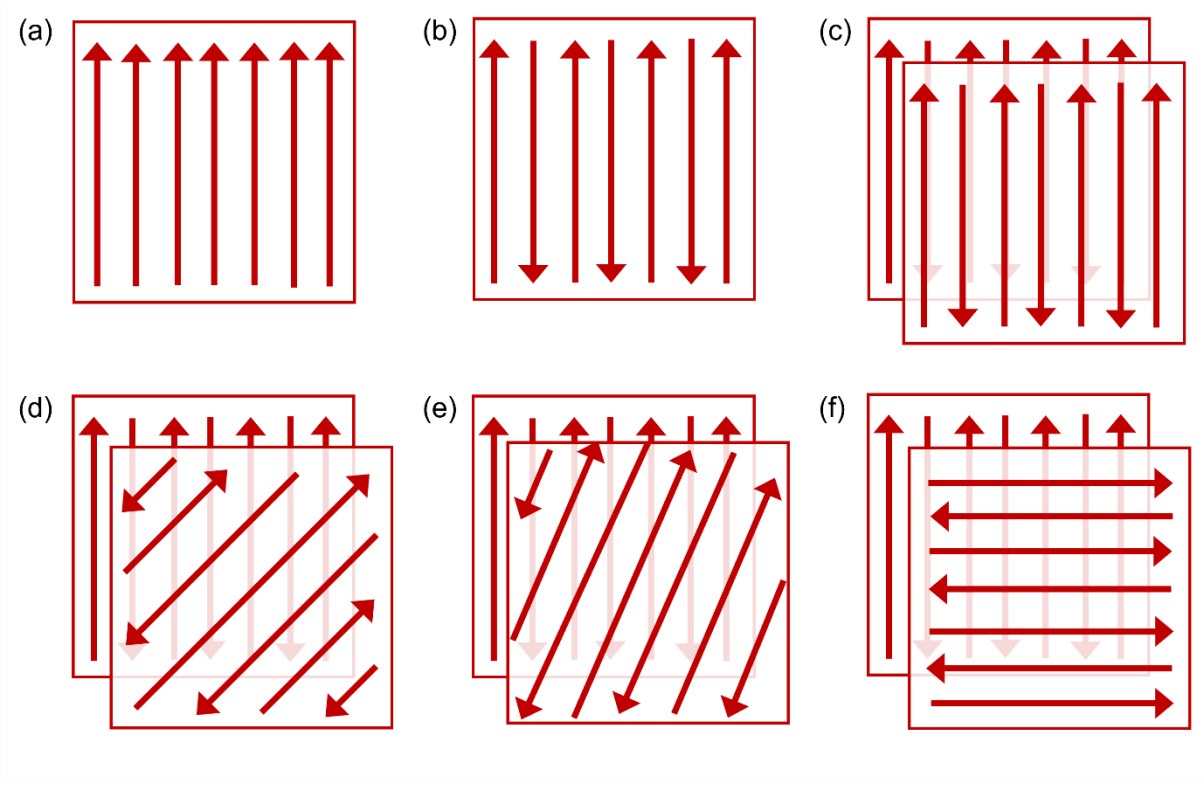

Figure 3: Schemetic of selected scan strategies in PBF-LB (a) Unidirectional scan strategy (b) Bidirectional scan strategy, (c) No scan rotation with bidirectional scan strategy, (d) Scan rotation of 45° with bidirectional scan strategy, (e) Scan rotation of 67° with bidirectional scan strategy, and (f) Scan rotation of 90° with bidirectional scan strategy.

4. Materials and methods

4.1. Materials

Fe-6.5 wt.% Si powder produced by gas atomization and supplied by Höganäs AB (Sweden) was used as the feedstock material for this study. The suitability of this powder for PBF-LB processing was first assessed through particle size analysis, which revealed a size range of approximately 10 to 45 µm. Subsequent morphological examination using scanning electron microscopy showed that particles largely exhibited a spherical geometry, consistent with gas-atomized feedstocks. To verify the chemical purity, elemental analysis was performed and confirmed the presence of elemental iron and silicon in the intended proportions, with no detectable contamination. In addition, X-ray diffraction measurements indicated that the powder consisted of a single-phase body-centered cubic (BCC) solid-solution structure.

4.2. PBF-LB processing

PBF-LB experiments were conducted in an EOS M100 system (EOS GmbH, Germany) using an ytterbium fiber laser with a maximum power of 200 W and a nominal spot size of 40 µm. All builds were performed under an argon atmosphere, with the oxygen levels maintained below 1000 ppm to reduce oxidation. In paper 1, a design-of-experiments approach was implemented for the process parameter studies by varying laser power (90 -170 W) and scan speed (600 -1400 mm/s) keeping a constant layer thickness of 0.02 mm and hatch distance of 0.06 mm. A bidirectional stripe scanning strategy with a 67° scan rotation, a stripe width of 5 mm, and a stripe overlap of 0.1 mm was used consistently across all builds. In Paper 2, the scan rotation was varied between 0°, 45°, 67°, and 90°. To enable high-throughput evaluation and a multiple parameter sets were incorporated into each specimen in both works.

4.3. Heat treatment

Annealing was performed on selected samples at 1150 °C under flowing argon with a heating rate of 15 °C/min, followed by furnace cooling. A holding time of 2 hours was used in Paper I, while the samples in Paper II were annealed for 1 hour.

4.4. Sample preparation

Printed specimens were sectioned along planes parallel to both the build direction and laser scanning direction for characterization and property measurements. These sections were utilized for relative density measurements, microstructural analysis, and Vickers hardness testing. Following sectioning, the samples were hot-mounted in a conductive resin to facilitate handling and conductive analysis.

Metallographic preparation was carried out using conventional grinding and polishing procedures. Grinding was performed sequentially with 500, 1000, and 2000 grit silicon carbide (SiC) papers, with each step lasting approximately 1-3 minutes. The surface was then polished for 5 minutes each using diamond suspensions with particle sizes of 3µm and 1µm. For EBSD measurements, an additional polishing step using colloidal silica (OP-S) was conducted to achieve a deformation-free surface. Chemical etching using a 2 % Nital solution was applied to selected samples to reveal the melt pool morphology.

For electrical resistivity and XRD measurements, cross-sectioned specimens with a thickness of ~1 mm were prepared. Magnetic measurements were performed on small samples weighing between 10 and 30 mg, which were shaped as close to cubic geometry as possible to minimize shape-related effects.

4.5. Optical Microscopy (OM) and relative density calculation

Optical microscopy was performed using a Zeiss Axioscope 7 microscope equipped with an automated motorized stage. The automated stage enabled the acquisition of multiple adjacent micrographs, which were subsequently stitched together to generate high-resolution images covering the entire sample cross-section. These large-area images were used for quantitative evaluation of relative density by capturing representative porosity distributions across the samples. Image analysis was performed using ImageJ software, where the images were binarized and the area fractions of the dense regions were taken as the relative density of the printed specimens.

4.6. Scanning Electron Microscopy (SEM)

Microstructural characterization was performed using a Gemini 450 Field Emission Scanning Electron Microscope (FEG-SEM) equipped with a Symmetry S3 Electron Back Scatter Diffraction (EBSD) detector (Oxford Instruments, Abingdon-on-Thames, UK). EBSD measurements were performed to obtain large-area orientation maps, which were acquired at a magnification of 150x using a step size of 1 µm. During data acquisition, the samples were tilted by 70° relative to the incident electron beam, and an accelerating voltage of 20 kV was used. A working distance of approximately 18 mm was maintained to optimize EBSD signal quality. The acquired EBSD data were processed and analyzed using AZtec Crystal software, which was employed for quantitative analysis of crystallographic orientation and microstructural features.

4.7. X-Ray Diffraction (XRD)

X-ray diffraction analysis was carried out using a Bruker D8 Discover diffractometer with Cu Kα radiation (λ = 1.5406 Å) to determine the phase constitution of the samples. Diffraction data was acquired in Bragg - Brentano geometry over a 2θ range of 25-90°, using a step size of 0.015° and a counting time of 1 s per step, ensuring sufficient angular resolution for accurate phase detection. The collected diffraction patterns were analyzed using Bruker DIFFRAC.EVA software, which was employed for background subtraction, peak identification, and comparison with reference diffraction data to determine the phase constitution of the samples.

For paper 2, a SAXSLAB Mat: Nordic system equipped with a Cu Kα radiation source (λ = 1.5406 Å) was used. The system is designed for high-throughput measurements, allowing automated sequential characterization of multiple samples by means of robotic handling, precise software-controlled alignment, and motorized positioning stages. Diffraction patterns were collected in the 2θ interval from 25° to 90° using a step size of 0.015° and an acquisition time of 1 s per step. Data processing and phase identification was carried out using Bruker DIFFRAC.EVA software.

4.8. Hardness testing

Vickers hardness measurements were performed using a StruersDurascan-70 G5 automated hardness tester to characterize the mechanical response of the samples. This setup was chosen to enable systematic and high-throughput characterization, featuring automated indentation and imaging capabilities. A test force of HV1 (1 kgf) was applied with a dwell time of 10 s, and the resulting indents were imaged at 20x magnification. 10 to 15 measurements were performed on each specimen by selecting random indentation locations in accordance with ASTM guidelines. The final hardness values were obtained by averaging the measurements, and standard deviation was reported to assess the consistency of results.

4.9. Vibrating Sample Magnetometer (VSM)

The magnetic properties of the samples were measured using a Vibrating Sample Magnetometer (Lake Shore Cryotronics 8600 series). The samples were mounted on a carbon fiber holder and the Hysteresis (M-H) loops were recorded by applying an external magnetic field of up to 1270 kA/m. Measurements were performed with build direction aligned both parallel and perpendicular to the applied magnetic field (H ∥ BD and H ⊥ BD respectively) in order to probe the directional magnetic behavior. Coercivity (Hc) and saturation magnetization (Ms) were determined from the M-H curves, with Ms defined as the magnetization measured

at 1270 kA/m. The mass magnetic susceptibility (χ_m) was determined from the slope of initial segment of the M-H curve.

4.10. Electrical property testing

To characterize the electrical properties, resistivity measurements were performed using a four-point probe system (CMT-SR2000N, Changmin Tech). In this method, electrical current is supplied through the two outer probes; while resulting voltage drop is measured across the inner probes, allowing the resistance of the material to be determined independently of probe contact effects. During the measurements, the probe assembly was oriented perpendicular to the build direction to maintain a consistent current path relative to the additively manufactured microstructure. The system directly records the resistance based on the applied current and measured voltage, after which electrical resistivity was calculated using Equation (2) [51, 52].

$$\rho = \frac{V}{I} \cdot \frac{\pi t}{\ln\left(\frac{\sinh(\frac{t}{s})}{\sinh(\frac{t}{2s})}\right)} \quad (2)$$

where V, I, t and s are voltage, current, sample thickness and probe spacing, respectively.

5. Summary of appended papers

The results presented in the appended papers are summarized in this section. In Paper 1, the effects of PBF-LB process parameters and post-processing heat treatment on microstructure and functional properties are explored, addressing RQ1 and RQ3. Paper 2 addresses RQ2 and RQ3, with a particular emphasis on the role of laser scan strategies and heat treatment in influencing microstructural and functional properties.

Paper 1: Energy density-driven microstructure and functional properties of Fe-6.5 wt.% Si steel processed by powder bed fusion-laser beam

The motivation for Paper 1 was to understand how the PBF-LB process parameters and the post-processing treatments affect the density, microstructure and properties of PBF-LB processed high-silicon steel.

A systematic investigation was carried out by exploring a broad range of laser power and scan speed combinations without build-platform heating, using a high-throughput approach. The results enabled the identification of distinct processing regimes associated with lack-of-fusion defects and keyhole porosity. An optimal process window yielding near-fully dense samples (>99% density) was identified (**Figure 4a**). Correlating the relative density with VED showed that the process window of 100 and 150 J/mm³ is good for the samples with optimal density (**Figure 4b**).

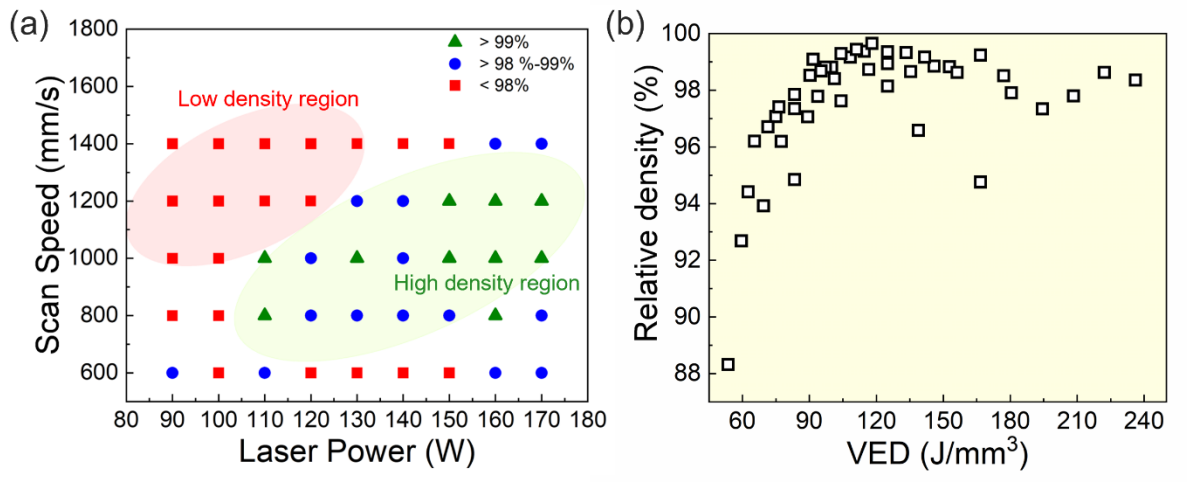

Figure 4:(a) Process window showing the distribution of relative density of as-printed Fe-6.5 wt.% Si samples. High density and low density regions are marked in green and red bubbles respectively. (b) Relative density of the samples as a function of volumetric energy density (VED).

The investigation of magnetic properties revealed a pronounced anisotropy as reflected in both coercivity and saturation magnetization (**Figure 5a**). Coercivity decreased with increasing VED, indicating the influence of solidification-induced texture development and grain morphology. In contrast, saturation magnetization showed no clear dependence on VED, suggesting that it is governed primarily by alloy composition rather than microstructural features or defects. Detailed analysis of some samples with relative densities exceeding 99% demonstrated progressive microstructural coarsening with increasing VED. Following annealing at 1150° C for 2 hours, grain growth and microstructural homogenization led to a substantial improvement in magnetic performance, with coercivity reduced by ~60-80% (**Figure 5b**). Overall, these results highlight the central role of VED in governing density, microstructure, and multifunctional anisotropy in PBF-LB processed high-silicon steel, providing a robust basis for selecting processing conditions suitable for high-performance soft magnetic components.

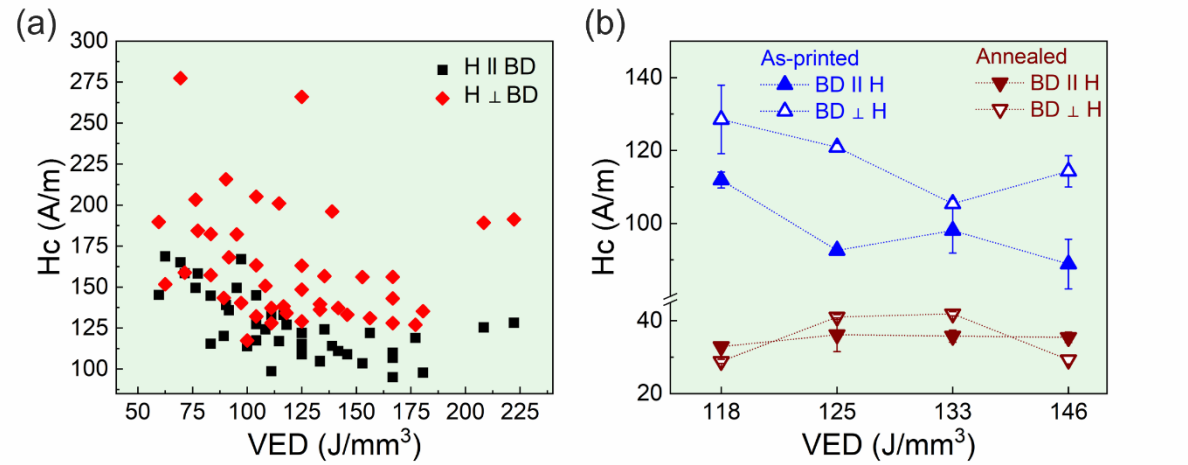

Figure 5: (a) Coercivity of as-printed Fe-6.5wt%Si samples as a function of VED measured with applied magnetic field (H) parallel (H ∥ BD) and perpendicular (H ⊥ BD) to the build direction (BD) (b) Coercivity of selected Fe-6.5wt%Si samples in as-printed and annealed conditions, measured in parallel and perpendicular directions, as a function of VED.

Paper 2: Laser path engineering of microstructure and multi-properties in additively manufactured high-silicon steel

After establishing a defect-free processing window with optimal magnetic performance in Paper 1, Paper 2 focuses on investigating the influence of laser scan strategies on the microstructure and multifunctional properties of PBF-LB processed high-silicon steel. In particular, the study examines how scan rotation angle and subsequent annealing affects the magnetic, mechanical, and electrical behavior of Fe-6.5 wt.% Si alloy.

Four different scan rotation angles (0°, 45°, 67°, and 90°) were incorporated within a single specimen to enable efficient sample preparation and characterization (**Figure 6a**). Melt pool analysis revealed that laser path rotation has a pronounced effect on melt pool morphology, even when hatch distance and layer thickness are held constant. A 0° rotation resulted in vertically aligned, deeply penetrating melt pools due to repeated re-melting, whereas the 45° and 90° rotations produced more heterogeneous melt pool arrangements. At a rotation angle of 67°, the melt pools exhibited a fully randomized orientation, confirming that interlayer re-melting patterns strongly depend on scan rotation.

These variations in melt pool morphology translated directly into distinct microstructural features (**Figure 6b**). The 90° scan rotation promoted the formation of coarse, elongated columnar grains with a strong ⟨001⟩ texture, which is beneficial for both magnetic and mechanical performance. In contrast, the 0° rotation produced narrower columnar grains with a high density of grain boundaries. The 45° and 67° rotations resulted in more heterogeneous microstructures characterized by mixed grain sizes and weaker textures. Annealing promoted recrystallization and grain growth, however, exhibit different degrees of recrystallization and grain growth in different samples which are reflected in the properties as well (**Figure 6c**).

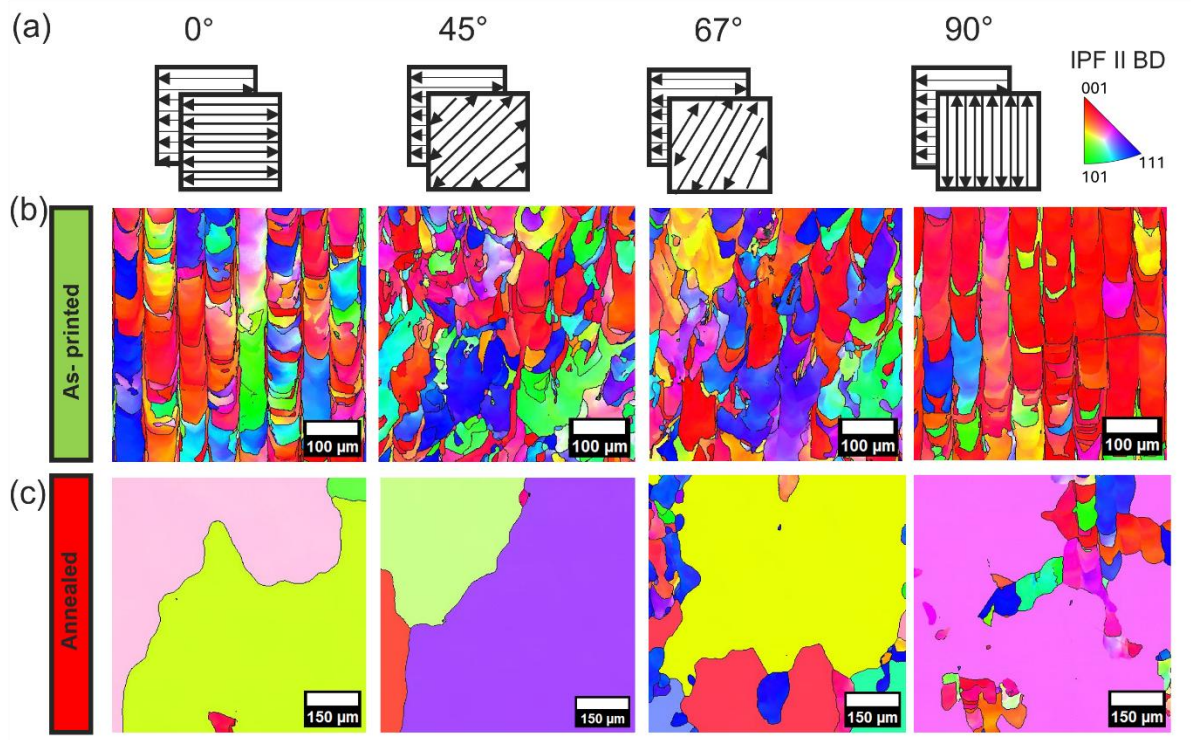

Figure 6: (a) Schematic of different scan rotation strategies used in the study. EBSD orientation maps (IPF coloring) of (b) as-printed and (c) annealed Fe-6.5 wt.% Si samples corresponding to different scan rotations, taken along the build direction.

Magnetic behavior in the as-printed samples has a dependence on corresponding rotation-dependent grain morphology. A 0° rotation produced narrow, irregular grains associated with higher coercivity, whereas the coarse and well-oriented columnar grains formed at 90° resulted in improved magnetic performance; 45° and 67° rotations showed intermediate responses due to more heterogeneous grain structures (**Figure 7a**). Annealing at 1150° C for 1 hour led to a substantial coercivity reduction of ~1.5–3.5 times for all rotations, most notably for the 0° condition (**Figure 7b**), while simultaneously reducing magnetic anisotropy through grain growth and microstructural homogenization. Across all conditions, superior soft magnetic properties were obtained when the magnetic field was applied parallel to the build direction because of reduced domain-wall pinning.

Vickers hardness measurements indicated a gradual decrease in hardness with increasing scan rotation angle in the as-printed condition, while annealed samples generally exhibited lower hardness due to grain coarsening (**Figure 7c**). An exception was observed for the 90° rotation after annealing, which showed partial recrystallization and a mixed grain size distribution. Electrical resistivity was highest for the 0° rotation sample in both conditions, reflecting its

fine grain structure, whereas the 45° and 67° rotation samples exhibited resistivity values close to the reported values of ~82 μΩ.cm for randomly oriented grains (**Figure 7d**).

These results demonstrate that laser scan rotation plays a critical role in controlling microstructure and multifunctional properties in PBF-LB processed high-silicon steel. Strategic adjustment of scan strategies, combined with appropriate heat treatment, enables effective tailoring of magnetic, mechanical, and electrical performance, offering a viable pathway for site-specific property control in next-generation energy-efficient electrical machines.

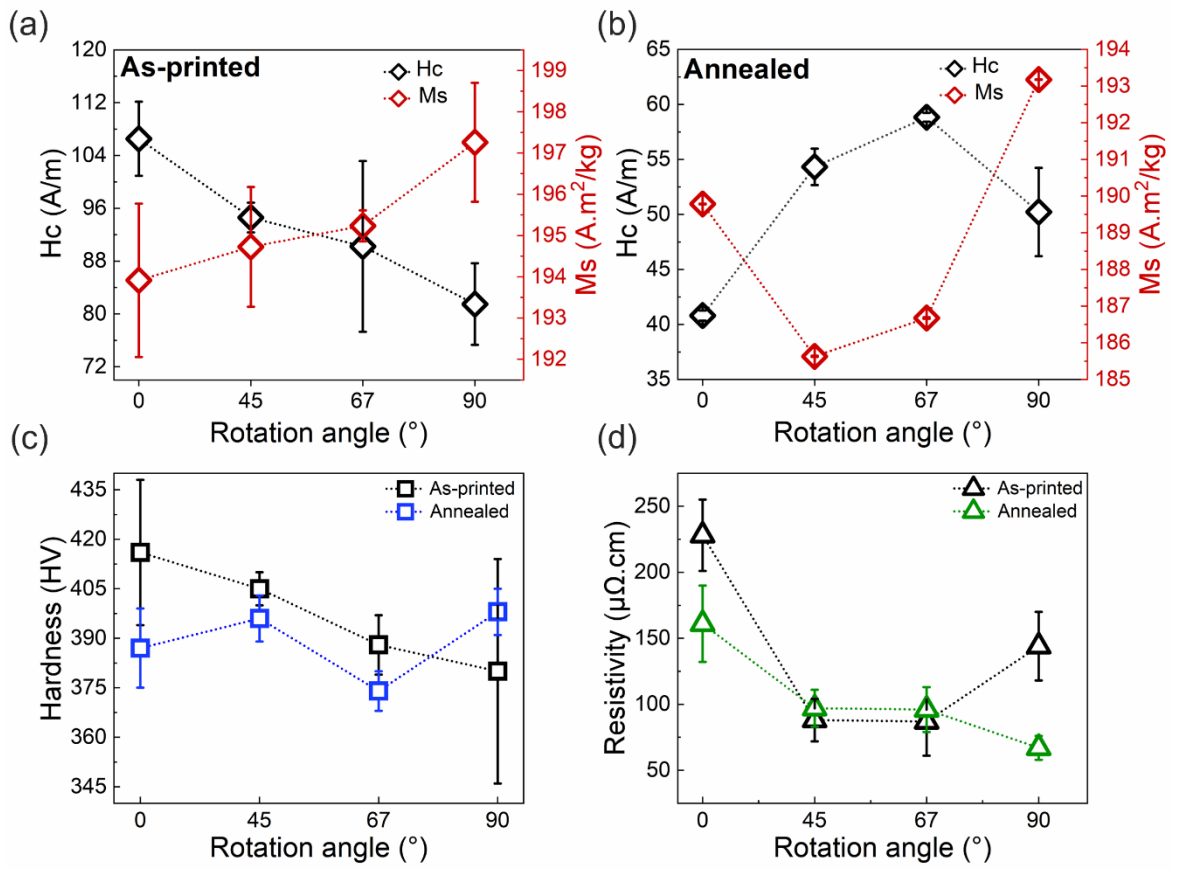

Figure 7: Variation of (a) coercivity and (b) saturation magnetization of Fe-6.5 wt.% Si samples with different scan rotation strategies in as-printed and annealed conditions. The measurements are performed with applied magnetic field parallel to build direction condition. Variation of (c) hardness and (d) electrical resistivity with different scan rotation angles for both the conditions. Measurements are taken from the surface parallel to the build direction.

6. Conclusions

The conclusions drawn from the work presented in this thesis are as follows:

RQ1: What is the effect of PBF-LB process parameters on the microstructure and functional properties (magnetic, mechanical and electrical properties) of Fe-6.5 wt.% Si alloys?

- In PBF-LB processed Fe–6.5 wt.% Si samples, relative density and magnetic performance showed a strong dependence on VED.
- At low VED values (< ~90 J/mm^3), lack-of-fusion porosity was dominant due to insufficient energy input to fully melt and consolidate the powder layer.
- At high VED values (> ~150 J/mm^3), keyhole porosity formed because of excessive energy input and vapor-induced melt pool instability.
- A stable processing window (with relative densities > 99%) was identified between 100-150 J/mm^3 where stable melting process occurred.
- Magnetic properties were found to vary with VED, with coercivity decreasing as VED increased, while saturation magnetization remained largely unchanged.
- Strong magnetic anisotropy observed in the as-printed condition originated from elongated grains aligned along the build direction.

RQ2: How do variations in laser scan strategies affect the microstructural evolution and functional properties of Fe-6.5 wt.% Si alloys?

- Laser scan rotation is identified as a key parameter controlling melt pool characteristics, grain structure and resulting magnetic, electrical, and mechanical responses in PBF-LB processed Fe-6.5wt.% Si.
- Melt pool analysis showed vertically aligned and deeply penetrating melt pools for 0°, heterogeneous arrangements at 45° and 90°, and fully randomized melt pool orientations at 67° scan rotation strategies.
- The 0° scan rotation favored the formation of fine columnar grains, whereas a 90° rotation promoted coarser elongated well-aligned grains with a preferred <001> texture. The 45° and 67° rotation gave rise to grains with heterogeneous morphologies and weaker preferred orientation.

- As-printed samples exhibited pronounced magnetic anisotropy resulting from elongated columnar grains aligned along the build direction and the associated crystallographic texture.
- The 0° scan rotation strategy resulted in higher coercivity whereas the 90° scan rotation led to enhanced soft magnetic properties (lower coercivity and higher saturation magnetization). At 45° and 67° rotations, intermediate soft magnetic behavior is observed.
- Hardness values varied with the scan rotation strategies, where 0° rotation exhibited the highest hardness and 90° scan rotation showed the lowest values.
- The 0° scan rotation exhibited exceptionally high electrical resistivity due to the narrower grain structures, whereas other scan rotation strategies showed the values close to those typically reported for conventionally processed Fe-6.5 wt.% Si alloys.

RQ3: What is the impact of post-processing on the microstructure and functional properties of Fe-6.5 wt.% Si alloys?

- Annealing effectively promoted recrystallization and grain growth, resulting in a more homogeneous grain structure.
- Magnetic anisotropy was largely eliminated following annealing, as grain growth reduced grain boundary density, thereby decreasing domain-wall pinning and enhancing the soft magnetic response.
- Coercivity decreased under all processing conditions after annealing, demonstrating that post-processing heat treatment strongly influences soft magnetic performance.

7. Future work

Based on the findings reported in this licentiate thesis, the following directions are recommended for future research relevant to the study's research questions:

- A comprehensive performance evaluation of Fe-Si prototypes manufactured using PBF-LB with optimized process parameters is needed. In particular, core loss measurements are important to assess functional performance. This includes printing prototypes using the best-performing parameter sets and systematically evaluating their magnetic loss characteristics.
- An in-depth investigation of texture evolution and ordered phase formation in PBF-LB processed Fe-Si alloys should be conducted. Advanced X-ray based characterization techniques could provide further insight into the relationship between processing conditions, microstructure, and functional properties.
- All samples in the present work were fabricated using a layer thickness of 20 μm. To improve productivity, future studies should examine the influence of increased layer thickness on microstructure and multifunctional properties.
- Cracking was observed in the printed samples, primarily due to residual stresses arising from the absence of build-platform heating. To mitigate crack formation and improve structural integrity, post-processing techniques such as Hot Isostatic Pressing (HIP) should be explored.

Acknowledgements

First and foremost, I would like to thank my supervisors, Assistant Prof. Varun Chaudhary and Prof. Eduard Hryha, for giving me the opportunity to pursue this PhD. I am grateful to them for their invaluable support, guidance, and feedback. I would also like to thank my examiner and division head, Prof. Uta Klement, for her assistance and feedback.

I would like to acknowledge the financial support from the Areas of Advance (AoA) in Production and Materials Science at Chalmers University of Technology.

I would like to acknowledge the Center for Additive Manufacture - Metal (CAM2), supported by the Swedish Governmental Agency of Innovation Systems (VINNOVA).

I would like to acknowledge Michal Starch from CMAL for their support, discussion, and assistance with XRD measurements.

I would like to thank Mattias Fredriksson from MC2 cleanroom lab for providing the four-point probe measurement setup facility.

I would also like to thank research engineers Antonio Mulone, Gowtham Soundarapandiyan, Dmitri Riabov, Eric Tam, Anders Bragée and Johnny Hamnesjö Olausson for their assistance with everything in AM lab, magnetic materials lab and chemistry lab.

I would also like to thank my colleagues Debottam Goswami, Sahith Kokkirala, Ahmed Fardan Jabir Hussain, Xiao Qin, Erika Tuneskog, Rasmus Gunnerek, Bala Malladi for fruitful discussions.

I would also like to thank MSc thesis students Akshay Shri Srinivas, Jayakrishnan Manalaya, Gokul Babu and Anthonius de Korte for their assistance in the work.

I would also like to thank all my dear colleagues at the Department of Mechanical Engineering, and specifically my colleagues in the Materials and Manufacture Division.

My heartfelt thanks to my parents, siblings and the rest of my family for their constant love and support throughout the years. I extend my heartfelt gratitude to all my teachers throughout my life for inspiring me to dream big.

Finally, I would like to thank my wife, Pooja, for her love and support during my good and bad days.

References

[1] Gutfleisch O, Willard MA, Brück E, Chen CH, Sankar SG, Liu JP. Magnetic Materials and Devices for the 21st Century: Stronger, Lighter, and More Energy Efficient. Advanced Materials. 2011;23:821-42.

[2] Guo Y, Liu L, Ba X, Lu H, Lei G, Yin W, et al. Designing High-Power-Density Electric Motors for Electric Vehicles with Advanced Magnetic Materials. World Electric Vehicle Journal2023. p. 114.

[3] Silveyra JM, Ferrara E, Huber DL, Monson TC. Soft magnetic materials for a sustainable and electrified world. Science. 2018;362:eaao0195.

[4] Ram BS, Paul AK, Kulkarni SV. Soft magnetic materials and their applications in transformers. Journal of Magnetism and Magnetic Materials. 2021/11/01;537.

[5] Krings A, Boglietti A, Cavagnino A, Sprague S. Soft Magnetic Material Status and Trends in Electric Machines | IEEE Journals & Magazine | IEEE Xplore. IEEE Transactions on Industrial Electronics. 2017;64.

[6] Ahmed N, Atkinson GJ. A Review of Soft Magnetic Composite Materials and Applications | IEEE Conference Publication | IEEE Xplore.

[7] Chaudhary V, Mantri SA, Ramanujan RV, Banerjee R. Additive manufacturing of magnetic materials. Progress in Materials Science. 2020;114:100688.

[8] Han L, Maccari F, Souza Filho IR, Peter NJ, Wei Y, Gault B, et al. A mechanically strong and ductile soft magnet with extremely low coercivity. Nature 2022 608:7922. 2022-08-10;608.

[9] Ouyang G, Chen X, Liang Y, Macziewski C, Cui J. Review of Fe-6.5 wt%Si high silicon steel—A promising soft magnetic material for sub-kHz application. Journal of Magnetism and Magnetic Materials. 2019;481:234-50.

[10] Rodriguez-Vargas BR, Stornelli G, Folgarait P, Ridolfi MR, Miranda Pérez AF, Di Schino A. Recent Advances in Additive Manufacturing of Soft Magnetic Materials: A Review. Materials2023. p. 5610.

[11] Bozorth RM. Ferromagnetism. Ferromagnetism1993. p. 1-968.

[12] Liu Y, Ma Z, Liu X, Wang Z, Zhang Z, Liu X. Ductile-to-brittle transition behavior of Fe-6.5 wt%Si alloy with three-point bending testing. Materials Characterization. 2023/06/01;200.

[13] Viala B, Degauque J, Fagot M, Baricco M, Ferrara E, Fiorillo F. Study of the brittle behaviour of annealed Fe-6.5 wt%Si ribbons produced by planar flow casting. Materials Science and Engineering: A. 1996/07/15;212.

[14] Namikawa M, Ninomiya H, Yamaji T. High silicon steel sheets realizing excellent high frequency reactor performance. JFE Tech Rep. 2005;6:12-7.

[15] Kasai S, Namikawa M, Hiratani T. Recent progress of high silicon electrical steel in JFE steel. JFE Tech Rep. 2016;21:14-9.

[16] Goll D, Schurr J, Trauter F, Schanz J, Bernthaler T, Riegel H, et al. Additive manufacturing of soft and hard magnetic materials. Procedia CIRP: Elsevier B.V.; 2020. p. 248-53.

[17] Périgo EA, Jacimovic J, García Ferré F, Scherf LM. Additive manufacturing of magnetic materials. Additive Manufacturing: Elsevier B.V.; 2019.

[18] Garibaldi M. Laser additive manufacturing of soft magnetic cores for rotating electrical machinery: materials development and part design. 2018.

[19] Herzog D, Seyda V, Wycisk E, Emmelmann C. Additive manufacturing of metals. Acta Materialia. 2016;117:371-92.

[20] Kosiba K, Gustmann T, Kim JT, Seok J, Jung J, Beyer L, et al. Experimental cooling rates during high-power laser powder bed fusion at varying processing conditions. Journal of Alloys and Compounds. 2023;967:171773.

[21] IEC 60404-1 Consolidated version. International Electrotechnical Commission (IEC).

[22] Lamichhane TN, Sethuraman L, Dalagan A, Wang H, Keller J, Paranthaman MP. Additive manufacturing of soft magnets for electrical machines—a review. Materials Today Physics. 2020;15:100255.

[23] Sarkar SK, Keskar N, Tan LP, Ingale T, Chesetti A, Dasari S, et al. A magnetically soft yet mechanically strong and ductile Ta free CoFeNi high entropy alloy with Al and Ti additions. Nature Communications. 2026;17:2890.

[24] Arai KI, Ishiyama K. Recent developments of new soft magnetic materials. Journal of Magnetism and Magnetic Materials. 1994;133:233-7.

[25] Herzer G. Soft magnetic nanocrystalline materials. Scripta Metallurgica et Materialia. 1995;33:1741-56.

[26] Fingers RT, Kozlowski G. Microstructure and magnetic properties of Fe-Co alloys. Journal of Applied Physics. 1997;81:4110-1.

[27] Sundar RS, Deevi SC. Soft magnetic FeCo alloys: Alloy development, processing, and properties. International Materials Reviews: IOM Communications Ltd.; 2005. p. 157-92.

[28] Yu RH, Basu S, Ren L, Zhang Y, Parvizi-Majidi A, Unruh KM, et al. High Temperature Soft Magnetic Materials: FeCo Alloys and Composites. IEEE Transactions on Magnetics2000. p. 3388-93.

[29] Herzer G. Modern soft magnets: Amorphous and nanocrystalline materials. Acta Materialia. 2013/02/01;61.

[30] Moses AJ. Electrical steels: past, present and future developments. IEE Proceedings A (Physical Science, Measurement and Instrumentation. 1990-9;137.

[31] He Y, Kestens LA, Youliang He LAK. The processing, microstructure, texture, and magnetic properties of electrical steels: A review. International Materials Reviews. 2024-8-21.

[32] Qin J, Yang P, Mao W, Ye F. Effect of texture and grain size on the magnetic flux density and core loss of cold-rolled high silicon steel sheets. Journal of Magnetism and Magnetic Materials. 2015;393:537-43.

[33] Füzer J, Birčáková Z, Zeleňáková A, Hrubovčák P, Kollár P, Predmerský M, et al. Investigation of total losses of non-oriented electrical steels. Acta Physica Polonica A. 2010;118:1018-9.

[34] Shimanaka H, Ito Y, Matsumura K, Fukuda B. Recent development of non-oriented electrical steel sheets. Journal of Magnetism and Magnetic Materials1982. p. 57-64.

[35] Cullity BD, Graham CD. Introduction to Magnetic Materials. Introduction to Magnetic Materials: Wiley; 2008.

[36] Shin JS, Bae JS, Kim HJ, Lee HM, Lee TD, Lavernia EJ, et al. Ordering-disordering phenomena and micro-hardness characteristics of B2 phase in Fe-(5-6.5%)Si alloys. Materials Science and Engineering: A. 2005;407:282-90.

[37] Swann PR, Grånäs L, Lehtinen B. The B2 and DO3 Ordering Reactions in Iron–Silicon Alloys in the Vicinity of the Curie Temperature. Metal Science. 1975;9:90-6.

[38] Dieter GE. Mechanical Metallurgy. 3rd edition ed. McGraw-Hill1961.

[39] Huadong F, Qiang Y, Zhihao Z, Jianxin X. Effects of precipitated phase and order degree on bending properties of an Fe-6.5 wt%Si alloy with columnar grains. Journal of Materials Research. 2011;26:1711-8.

[40] Gibson I, Rosen D, Stucker B. Additive manufacturing technologies: 3D printing, rapid prototyping, and direct digital manufacturing, second edition: Springer New York; 2015.

[41] Frazier WE. Metal additive manufacturing: A review. Journal of Materials Engineering and Performance: Springer New York LLC; 2014. p. 1917-28.

[42] Sun S, Brandt M, Easton M. 2 - Powder bed fusion processes: An overview. In: Brandt M, editor. Laser Additive Manufacturing: Woodhead Publishing; 2017. p. 55-77.

[43] Oliveira JP, LaLonde AD, Ma J. Processing parameters in laser powder bed fusion metal additive manufacturing. Materials & Design. 2020;193:108762.

[44] Thijs L, Verhaeghe F, Craeghs T, Humbeeck JV, Kruth J-P. A study of the microstructural evolution during selective laser melting of Ti–6Al–4V. Acta Materialia. 2010;58:3303-12.

[45] Buhairi MA, Foudzi FM, Jamhari FI, Sulong AB, Radzuan NAM, Muhamad N, et al. Review on volumetric energy density: influence on morphology and mechanical properties of Ti6Al4V manufactured via laser powder bed fusion. Progress in Additive Manufacturing. 2023;8:265-83.

[46] Dar J, Ponsot AG, Jolma CJ, Lin D. A review on scan strategies in laser-based metal additive manufacturing. Journal of Materials Research and Technology. 2025;36:5425-67.

[47] Haines M, List F, Carver K, Leonard D, Plotkowski A, Fancher C, et al. Role of scan strategies and heat treatment on grain structure evolution in Fe-Si soft magnetic alloys made by laser-powder bed fusion. Additive Manufacturing. 2022/02/01;50.

[48] Leicht A, Yu C-H, Luzin V, Klement U, Hryha E. Effect of scan rotation on the microstructure development and mechanical properties of 316L parts produced by laser powder bed fusion. Materials Characterization. 2020;163:110309.

[49] Sun SH, Hagihara K, Nakano T. Effect of scanning strategy on texture formation in Ni-25 at.%Mo alloys fabricated by selective laser melting. Materials and Design. 2018;140:307-16.

[50] Hofmann R, Käß M, Werz M, Weihe S. Optimization and Development of scanning strategies in PBF-LB/M - Influencing mechanical properties of additive manufactured parts. Procedia Structural Integrity. 2026;77:237-47.

[51] Tan LP, Padhy SP, Tsakadze Z, Chaudhary V, Ramanujan RV. Accelerated property evaluation of Ni–Co materials libraries produced by multiple processing techniques. journal of materials research and technology. 2022;20:4186-96.

[52] Tan LP, Chaudhary V, Tsakadze Z, Ramanujan RV. Rapid multiple property determination from bulk materials libraries prepared from chemically synthesized powders. Scientific Reports. 2022;12:9504.